A MODEL FOR NON-VOLATILE FISSION PRODUCT RELEASE DURING REACTOR ACCIDENT CONDITIONS

B.J. LEWIS,* B. ANDRE AND G. DUCROS
Commissariat à l'Energie Atomique, Centre d'Etudes Nucléaires de Grenoble
Département de Thermohydraulique et de Physique, Service d'Etudes du Comportement du Combustible, 17 rue des Martyrs, 38054 Grenoble Cedex 9, FRANCE

D. MARO
Commissariat à l'Energie Atomique, Centre d'Etudes Nucléaires de Fontenay aux Roses
Institut de Protection et de Sûreté Nucléaire, Département de Protection de l'Environnement et des Installations, Service d'Etudes sur les Accidents, BP6, 92265 Fontenay aux Roses, FRANCE

ABSTRACT

An analytical model has been developed to describe the release kinetics of non-volatile fission products (e.g., Mo, Ce, Ru and Ba) from uranium dioxide fuel under severe reactor accident conditions. The present treatment considers the rate-controlling process of release in accordance with diffusional transport in the fuel matrix and fission product vaporization from the fuel surface into the surrounding gas atmosphere. The effect of the oxygen potential in the gas atmosphere on the chemical form and volatility of the fission product is considered. A correlation is also developed to account for the trapping effects of Sb and Te in the Zircaloy cladding.

This model has been used to interpret the release behaviour of fission products observed in the CEA experiments conducted in the HEVA/VERCORS facility at high temperature in a hydrogen and steam atmosphere.

1. INTRODUCTION

During a severe reactor accident, fission products will be released from the degraded core. The amount of release will depend on various physical and chemical processes that occur in the fuel matrix and in the surrounding atmosphere. The release kinetics of the volatile fission products (Xe, Kr, Cs and I) can be described by a rate-limiting process of solid-state diffusion through the UO_2 fuel matrix.[1,2,3,4] On the other hand, vaporization from the fuel surface is the governing mechanism of release for the relatively involatile species (Sr, Y, Zr, Nb, Mo, Tc, Ru, Rh, Pd, Ba, La, Ce, Pr and Nd).[5,6,7,8,9,10] This second process will depend directly on the vapor pressure of the fission product and on the subsequent mass transfer from the fuel surface to the gas stream that flows past the fuel. It may also involve chemical reactions of the fission product with the gaseous environment.

Since high temperatures are experienced during a severe reactor accident, chemical equilibrium can be assumed for the determination of the chemical form of the fission product. The speciation will depend directly on the oxygen potential of the gas environment, which can change as a result of hydrogen

---

* *Visiting scientist from the Royal Military College of Canada, Department of Chemistry and Chemical Engineering, Kingston, Ontario, CANADA K7K 5L0.*

production from steam oxidation of structural materials (i.e., Zircaloy) within the damaged core. The free energy of formation of various fission product oxides are shown as an Ellingham diagram in Fig. 1.[6,11,12,13] The most stable oxides (e.g., Ce_2O_3 and La_2O_3) are formed at low oxygen potentials; also quite stable are BaO, SrO and Eu_2O_3. Oxides requiring relatively high potentials include the species TeO_2, Sb_2O_3 and RuO_4. The range of the oxygen potential in the gas atmosphere anticipated in a typical reactor accident is shown in Fig. 1 for a partial pressure ratio of hydrogen-to-steam of 0.1 to 10. Within this range, oxides are expected to form for the La, Eu, Sr and Ba fission products, whereas metals will form for the Ru, Te and Sb products.

The chemical form (metal versus oxide) of the fission product can significantly affect its volatility.[6] For example, in the Vertical Induction (VI) tests at the Oak Ridge National Laboratory (ORNL), small releases of barium and europium have been observed in a steam environment where these products occur as low-volatility oxides in the fuel (BaO and Eu_2O_3). In comparison, higher releases were observed in a hydrogen atmosphere, under similar temperature conditions, in which higher-volatility metallics may have formed.[1,14]

In the present work, an analytical model is developed to describe the non-volatile release behaviour. This physical model is based on mass transfer considerations.[5,10] The present treatment also employs the results of an earlier determination of the fission-product vapor pressure based on a free energy minimization calculation for a system consisting of a condensed phase (UO_2 plus fission products) and a gas phase (H_2O and H_2 plus gaseous fission product species).[7-9] The model is validated against non-volatile release data measured in high-temperature, annealing experiments, conducted in both hydrogen and steam, as part of the HEVA/VERCÓRS test program at the Commissariat à l'Energie Atomique (CEA).[15]

2. MODEL DEVELOPMENT

The release of fission products from the damaged fuel rod occurs as a two-step process, consisting of: (i) transport through the fuel matrix, and (ii) vaporization into the gas stream flowing past the rod. Thus, the release kinetics are controlled by the rate-limiting step. As discussed in Section 1, the first process is the slower one for the volatile species; in contrast, the second process becomes rate-limiting for the non-volatile products. These mechanisms are described mathematically in the following sections.

2.1 Fission-Product Transport Through Fuel Matrix

As detailed in Ref. 4, fission-product transport in the uranium dioxide fuel matrix can be described by a generalized diffusional release process. The release fraction (in the case of no fission product trapping in the fuel porosity) is given by:

$$F = \frac{N_d(\tau)}{N_{go}} = F_d(\tau), \qquad (1)$$

where $N_d(\tau)$ is the number of atoms which has diffused through the solid matrix and N_{go} is the original inventory in the fuel at time t = 0. The function $F_d(\tau)$ is given by a transformed Booth relation:[4]

$$F_d = \begin{cases} 6\sqrt{\frac{\tau}{\pi}} - 3\tau, & for\ \tau \leq 0.1, \\ 1 - \frac{6}{\pi^2}\exp\{-\pi^2\tau\}, & for\ \tau > 0.1. \end{cases} \tag{2}$$

The dimensionless variable τ is evaluated from the integral relation

$$\tau = \int_0^t D'(t)\,dt \approx \sum_0^t D'(t)\Delta t, \tag{3}$$

in which $D' = D/a^2$, D is the diffusion coefficient (in m^2/s) and a is the grain radius (in m).

Equation (3) accounts for a time-variable diffusivity that depends directly on the temperature T and on the stoichiometry deviation x in UO_{2+x} as the fuel oxidizes in steam. The diffusion coefficient $D(x,T)$ for the volatile cesium species is given in Ref. 4. The calculation of the fuel oxidation kinetics in a variable hydrogen/steam gas mixture is also detailed in this reference. The oxygen potential curves (in kJ/mol O_2) shown in Fig. 1 for hyperstoichiometric fuel (UO_{2+x}) can be calculated from the Blackburn thermochemical model:[4,16]

$$\Delta\bar{G}_{O_2} = RT\ln(p_{O_2}) = RT\ln\left\{\left(\frac{x(2+x)}{(1-x)}\right)^2 k\right\}, \tag{4}$$

where $\ln k = 108x^2 - 32700/T + 9.92$, R is the ideal gas constant (= 8.314×10^{-3} kJ mol^{-1} K^{-1}), T is the temperature (in K) and p_{O2} is the oxygen partial pressure (in atm). Similar curves in Fig. 1 for a gas mixture in the atmosphere (as a function of the partial pressure ratio of hydrogen-to-steam (p_{H_2}/p_{H_2O})) can be evaluated from the Wheeler and Jones formulation:[4,17]

$$\Delta\bar{G}_{O_2} = RT\ln p_{O_2} = RT\left[-\frac{57625}{T} + 4.509\log T - 2.224 - 4.605\log\left(\frac{p_{H_2}}{p_{H_2O}}\right)\right]. \tag{5}$$

The equilibrium stoichiometry deviation of the fuel for a given fuel temperature is simply evaluated on equating Eqs. (4) and (5), i.e., as indicated by the intersection of the corresponding oxygen potential lines for the fuel and atmosphere in Fig. 1.

2.2 Fission-Product Vaporization

The vaporization release of non-volatile fission products from the fuel depends on the the partial vapor pressure of the material and the mass transfer from the fuel surface into the carrier gas stream. From mass transfer theory, the release rate (R_i) (in atom/s) of a fission product species i, from an exposed fuel surface area (S) (in m^2), is given:[5,18]

$$R_i = S\gamma_i N_A\{k_{im}(x_{is} - x_{i\infty})\}, \tag{6}$$

where k_{im} is the mass transfer coefficient (see Section 2.2.1) (mol m^{-2} s^{-1}), x_{is} is the mole fraction of fission product i at the surface of the fuel, $x_{i\infty}$ is the mole fraction of fission product i in the bulk gas stream, γ_i is the number of atoms per molecule of fission product i, and N_A is Avogadro's number (= 6.022 x 10^{23} mol^{-1}). The mole fraction of fission product at the surface of the fuel is

$$x_{is} = p_{iv}/p_T, \tag{7}$$

where p_{iv} is the partial pressure (in atm) of the fission product i in the vapor phase (see Section 2.2.2), and p_T is the total system pressure (= 1 atm in the present analysis). For the small quantities of non-volatile fission products anticipated in the bulk stream, it can be assumed that $x_{i\infty} \approx 0$.

Depending on the chemical form of the fission product as a result of the atmospheric conditions (e.g., metal versus oxide) (see Section 1), the species may be sufficiently volatile that the rate of release is dominated by mass transport through the solid fuel. The rate-controlling step (solid-state diffusion versus vaporization) can be determined from mass-balance considerations. At a given time t, the number of atoms in a condensed phase (liquid or solid) on the fuel surface, $N_c(t)$, is equal to the number atoms that diffuse to the surface, $N_d(t)$, (see Eq. (1)) minus the amount which is released by vaporization, $N_r(t)$, i.e.,

$$N_c(t) = N_d(t) - N_r(t), \tag{8}$$

where, using Eq. (6) (and dropping the subscript i):

$$N_r(t) = \int_0^t R(t')\,dt'. \tag{9}$$

Obviously, if $N_d \leq N_r$ in Eq. (8), there is an insufficient release to the fuel surface to keep up with the vaporization (i.e., N_c must be $\geq$ 0) and, therefore, the release kinetics will be dictated by the diffusional process of Eq. (1).

2.2.1 Mass Transfer Coefficient. Using a heat/mass transfer analogy, the mass transfer coefficient k_m (dropping the subscript i) in Eq. (6) for a cylinder fuel specimen can be determined using correlations for annular flow, i.e., in the case of a forced-convective carrier gas flow in the laminar regime (see Section 3):[18,19]

$$Nu_{AB} = \frac{k_m D}{c Đ_{AB}} = \begin{cases} 1.62\,(ReScD/L)^{1/3} & \text{for } L/(DReSc) < 0.07, \\ 4 & \text{for } L/(DReSc) \geq 0.07, \end{cases} \tag{10}$$

where Nu_{AB} is the Nusselt number for mass transfer, Re is the Reynolds number = $DV\rho/\mu$, Sc is the Schmidt number = $\mu/(\rho Đ_{AB})$, D is the equivalent diameter = $D_1 - D_2$ (m), D_1 is the channel diameter = 25 x 10^{-3} m (see Section 3), D_2 is the fuel rod diameter = 9.5 x 10^{-3} m (see Section 3), L is the fuel rod length = 80 x 10^{-3} m (see Section 3), c is the molar concentration of gas around the fuel specimen = $p_T/(RT)$, $Đ_{AB}$ is the binary diffusion coefficient of fission product (A) in carrier gas (B) (m^2/s), V is the bulk flow velocity (m/s), ρ is the bulk gas density (kg/m^3), and μ is the bulk gas viscosity (kg m^{-1} s^{-1}).

The bulk gas density ρ can be evaluated using an ideal gas law

$$\rho = \frac{p_T M}{RT}, \tag{11}$$

where p_T is the system pressure (= 1.013×10^5 N/m^2) and M is the molecular weight of the carrier gas. For a gas mixure, M can be evaluated from

$$M = \sum_i x_i M_i, \tag{12}$$

where i refers to the gas component and x_i is the mole fraction in the atmospheric mixture. The bulk gas viscosity μ (in g cm^{-1} s^{-1}) is calculated from[18]

$$\mu = 2.6693 \times 10^{-5} \frac{\sqrt{MT}}{\sigma^2 \Omega_\mu}, \tag{13}$$

where T is in K, M is in g/mol, and σ is the collision diameter of the molecule in the gas (in Å). The parameter Ω_μ can be determined from the expression $\Omega_\mu = 1/\{0.6441 + 0.2581 \ln(\kappa T/\epsilon)\}$ (i.e., this relation is derived from the values in Table 9-1 of Ref. 20), where ϵ/κ is a characteristic temperature (in K) of interaction between the molecules of the carrier gas. The values of σ and ϵ/κ for various carrier gases are given in Table 1. Similarly, for a gas mixture[18]

$$\mu = \sum_{i=1}^{n} \frac{x_i \mu_i}{\sum_{j=1}^{n} x_j \Phi_{ij}}, \tag{14}$$

in which

$$\Phi_{ij} = \frac{1}{\sqrt{8}} \left(1 + \frac{M_i}{M_j}\right)^{-1/2} \left[1 + \left(\frac{\mu_i}{\mu_j}\right)^{1/2} \left(\frac{M_j}{M_i}\right)^{1/4}\right]^2 . \tag{15}$$

Here n is the number of chemical species in the mixture, and the subscripts i and j correspond to the species i and j. The quantity Φ_{ij} is dimensionless and equals unity when $i = j$.

Finally, the binary diffusion coefficient $\mathcal{D}_{AB}$ (in cm^2/s), as needed for the calculation of the Schmidt number, can be evaluated from the Chapman-Enskog kinetic theory:[18,20,21]

$$\mathcal{D}_{AB} = 0.0018583 \frac{\sqrt{T^3 \left(\frac{1}{M_A} + \frac{1}{M_B}\right)}}{p_T \sigma_{AB}^2 \Omega_{\mathcal{D}_{AB}}}, \tag{16}$$

where T is in K, M is in g/mol, σ_{AB} is in Å, and the parameter $\Omega_{Ð_{AB}} = 1/\{0.7049 + 0.2910 \ln(\kappa T/\epsilon_{AB})\}$ (i.e., this relation is derived from the values in Table 11-1 of Ref. 20). The combining laws for the parameters σ_{AB} and ϵ_{AB} are based on the individual quantities for the fission product (A) and carrier gas (B) species such that:[21]

$$\sigma_{AB} = \frac{1}{2}(\sigma_A + \sigma_B)\,\xi^{-1/6}, \tag{18}$$

$$\epsilon_{AB} = \sqrt{\epsilon_A \epsilon_B}\,\xi^2. \tag{17}$$

The parameter ξ is a correction factor to account for the diffusion of a nonpolar-polar gas pair; for example, this factor would arise if a nonpolar fission product is diffusing in a polar steam medium. In this case,

$$\xi = 1 + \frac{1}{\sqrt{2}}\left(\frac{\alpha_n t_p^*}{\sigma_n^3}\right)\sqrt{\frac{\epsilon_p}{\epsilon_n}}, \tag{19}$$

where the subscripts n and p refer to the nonpolar and polar constituents. Here, α_n is the polarizability of the nonpolar molecule (e.g., see pg. 10-197 in Ref. 22), and

$$t_p^* = \frac{1}{\sqrt{8}}\frac{\mu_{dipole}^2}{\epsilon_p \sigma_p^3}, \tag{20}$$

where μ_{dipole} is the dipole moment of the polar gas. As shown in Table 3.10-1 of Ref. 21, $t_p^* = 1.2$ for steam. In the case of a nonpolar-nonpolar gas pair, ξ is simply equal to unity. If a trace fission product species is diffusing in a carrier gas mixture[18]

$$\frac{1}{Ð_{AB}} = \sum_{j=1}^{n} \frac{x_j}{Ð_{Aj}}, \tag{21}$$

where j refers to the components of the gas mixture.

Values of σ_A and ϵ_A are not known for many fission product species. These parameters, however, can be estimated from normal boiling point (subscript b) data, or from melting point (subscript m) data, according to[18]

$$\begin{aligned} \epsilon/\kappa &= 1.15\,T_b, & \sigma &= 1.166\,V_b^{1/3}\ (\mathit{liquid}), \\ \epsilon/\kappa &= 1.92\,T_m, & \sigma &= 1.222\,V_m^{1/3}\ (\mathit{solid}). \end{aligned} \tag{22}$$

For these empirical relations, ϵ/κ and T are in K, σ is in Å, and V (in cm^3/mol) is the molar volume of the liquid at the boiling point, or the molar volume of the solid at the melting point. The molar volume V_b in Eq. (22) can also be evaluated from the normal boiling temperature (T_b):[20]

$$T_b = \frac{\theta}{V_b^{0.18}} \exp\left(\frac{2.77\ V_b^{0.18}}{\theta} - 2.94\right), \tag{23}$$

where $\theta = T_b/T_c$. Here the critical temperature T_c can be evaluated as:[20]

$$T_c = 1.47\ T_b^{1.03}. \tag{24}$$

Using Eqs. (22), (23) and (24), the collision diameter can therefore be evaluted as a function of T_b (see Fig. 2). For example, values estimated from Fig. 2 for the noble gas species and for simple polyatomic substances have an average error difference of about 4% from those values reported in Ref. 18. The largest error in the calculation of the binary diffusion coefficient in Eq. (16) arises from the uncertainty in σ_{AB} as a result of the square dependence. However, this error becomes less significant in the present analysis because of the relative insensitivity of σ in Fig. 2 at higher boiling temperatures, i.e., typical of the involatile fission product species (where $T_b > 2000$ K).

2.2.2 Fission-Product Vapor Pressure. The total equilibrium pressure of the fission product (FP) vapor species has been reported for: the refractories (Zr, Nb, Tc, Ru, Rh and Pd);[7] and the lanthanides (La, Ce, Pr, Nd) as well as Sr, Y, and Ba.[9] The molybdenum has a much more complex behaviour (see discussion below) than the other refractory elements which have a stable chemical form as either an oxide or metal.[7,9]

The vapor pressures were determined from a free energy minimization treatment using the SOLGASMIX program.[7,9] The vaporization equilibrium was evaluated as a function of temperature (1000 to 3000 K), for total system pressures of 3 atm and 170 atm, and partial pressure ratios of H_2/H_2O in the gas atmosphere of 0.1, 1 and 10. This analysis was applied to systems containing a condensed phase (UO_2 plus FP) and a gas phase (H_2O and H_2 plus gaseous FP species). The total pressure of a specific FP was then evaluated as a function of temperature and gas phase chemical conditions (see Figs. 3 through 5). The chemical form of the fission product is therefore directly considered in terms of the atmospheric conditions. Simplified equations of the vapor pressure curves (except for Mo) are also given in Figs. 3(b) and 4(b). These equations are able to represent the curves in Figs. 3(a) and 4(a) within about 0.2 log units (factor of ~2). The amounts of fission products present in the fuel were based on an ORIGEN calculation for a commercial reactor at burnups of 37000 and 42800 MWd/tU (see Table 2), i.e., the reported vapor pressures can be scaled accordingly for different burnups.

The vapor pressure curves in Figs. 3 through 5 are for a total system pressure of 3 atm (the corresponding curves for 170 atm are given in Refs. 7 and 9). For most species, the vapor pressure is relatively insensitive to the H_2/H_2O ratio. The treatment for molybdenum, however, is more complex (see Fig. 5), which is related to the fact that the equilibrium chemical state for Mo can change from MoO_2 (in solid solution in UO_2) to metallic Mo as a function of temperature and the H_2/H_2O ratio. In addition, the vaporization of Mo depends strongly on the pressure of Cs in the vapor state due to the stable gaseous species Cs_2MoO_4; at higher temperatures, this species becomes less stable than CsOH and therefore does not contribute significantly.

3. COMPARISON OF MODEL TO EXPERIMENT

The non-volatile release model can be applied to annealing experiments conducted in the HEVA/VERCORS facility at the CEA. A brief description of the HEVA-6 and VERCORS-2 experimental conditions are given in Section 3.1. The model is compared to the experimental results in Section 3.2.

3.1 Experimental Description

Several high-temperature annealing tests were conducted at the CEA under atmospheric pressure in hydrogen (HEVA-6) and steam (VERCORS-2). The details of the fuel specimen, pretest irradiation conditions and experimental parameters are briefly summarized in Table 3. A schematic diagram of the experimental facility is shown in Fig. 6.

The fuel specimens were cut from spent commercial rods, and consisted of three pellets contained in the original Zircaloy cladding. A half-pellet of depleted UO_2 was placed at each end of the fuel stack, which was held in place by crimping the ends of the cladding (i.e., no end caps were used). The total fissile height was about 45 mm and the total sample height was ~80 mm. In order to restore the short-lived inventory after the long cooldown periods, the fuel samples were reirradiated in the SILOE experimental reactor for ~6 days at 8 W/cm for the HEVA test and at 15 W/cm for the VERCORS test.

In the HEVA-6 experiment (see Table 3 and the temperature history in Fig. 7), an initial phase was performed to oxidize the Zircaloy cladding; here, the fuel specimen experienced a mixture of steam (25 mg/s) and hydrogen (0.2 mg/s) at a temperature of ~1570 K for 60 min. The sample was then exposed to a reducing atmosphere of helium (8 mg/s) and hydrogen (0.2 mg/s) and ramped in temperature (1.4 K/s), where it was maintained at a high-temperature level of 2320 K for ~30 min.

The VERCORS-2 experiment (see Table 3 and the temperature history in Fig. 8) was carried out at a low-temperature plateau of ~1780 K for 30 min in a gas flow mixture of steam (25 mg/s), hydrogen (0.05 mg/s) and helium (0.5 mg/s). The fuel was then ramped in temperature (1.6 K/s), and experienced a high-temperature level of ~2100 K in a predominantly oxidizing atmosphere of steam (25 mg/s) and hydrogen (0.5 mg/s) for 13 min.

3.2 Model Application

3.2.1 HEVA-6 Test Analysis. The measured release kinetics of the relatively volatile species (i.e., ^{137}Cs, ^{131}I and ^{140}Ba) are shown in Fig. 7. As discussed in Ref. 4, the cesium release is dominated by diffusional transport in the fuel matrix, in accordance with Eqs. (1) through (3). The similar behaviour of the other fission products suggest that they are also controlled by diffusion, with a comparable diffusion coefficient (see discussion below for Ba). The end-of-test release fractions for these and other fission products are given in Table 4.

Since Fig. 7 indicates that there is no significant diffusional release at lower temperatures, one need only to consider an analysis for the high-temperature plateau region (where T ~ 2320 K). During this period, the given input flow rates correspond to partial pressures in the gas atmosphere of p_{He} = 0.9524 atm, p_{H2} = 0.04762 atm and p_{H2O} = 2.000 x 10^{-5} atm. This calculation assumes that the carrier gas (He and H_2) has an impurity level of 20 ppm of water vapor.[4] The oxygen potential in the atmosphere can be calculated using Eq. (5), where $p_{H2}/p_{H2O} \approx 2380$ and $T = 2320$ K. As shown in Fig. 1, the fission product Ba should be found as an oxide, whereas Ru will remain as a metal.

The flow conditions in the experiment (see Section 2.2.1) can be estimated as follows. The carrier gas primarily consists of He (mole fraction of ~95%), and therefore the bulk properties can be determined for this species. Equation (11) yields a density of $\rho = 2.1 \times 10^{-2}$ kg/m^3. Using Eq. (13), with the parameters for helium in Table 1, gives a viscosity of $\mu = 7.9 \times 10^{-5}$ kg m^{-1} s^{-1}. The bulk flow velocity can be determined from the relation:

$$V = \frac{m_f}{\rho A_c}. \tag{25}$$

For a mass flow $m_f = 8 \times 10^{-6}$ kg/s, and cross-sectional flow area $A_c = (\pi/4)[D_1^2 - D_2^2] = 4.20 \times 10^{-4}$ m^2, Eq. (25) gives $V = 0.91$ m/s. Using an equivalent diameter of $D = D_1 - D_2 = 1.55 \times 10^{-2}$ m, the Reynolds number is calculated as $Re = DV\rho/\mu = 3.7$, which indicates a laminar flow regime.

The vaporization rate of fission products can now be estimated having established the flow regime. As a typical example, consider the fission product Ba. As discussed previously, this species is presumably in oxide form (BaO), which has a boiling temperature of $T_b \sim 3200$ K.[5] Hence, Eq. (22) and Fig. 2 yield molecular force constants of $\epsilon_A/\kappa = 3680$ K and $\sigma_A = 6.0$ Å. Using Eqs. (16) to (18) (with $\xi = 1$), and the data in Table 1 for helium, one obtains $Ð_{AB} = 8.3 \times 10^{-4}$ m^2/s and a Schmidt number of $Sc = \mu/(\rho Ð_{AB}) = 4.6$. The quantity $(L/D)(Re\ Sc)^{-1}$ in Eq. (10) is evaluated as 0.30, and therefore $Nu_{AB} = 4$. Thus, the mass transfer coefficient in Eq. (10) is calculated to be $k_m = 1.1$ mol m^{-2} s^{-1} with the use of the relation $c = p_T/(RT)$. The vaporization rate follows directly from the release rate expression in Eq. (6). Using the simplified vapor pressure equation for Ba in Fig. 4 ($p_v = 1.48 \times 10^{-3}$ atm), and a fuel surface area of $S = 3.77 \times 10^{-4}$ m^2 (see Table 3), $R = 3.8 \times 10^{17}$ atom/s. Given that this constant release rate will occur over the 30-min temperature plateau, Eq. (9) yields a total release from the fuel specimen of $N_r = 6.8 \times 10^{20}$ atom. This value is greater than the original inventory in the fuel specimen (see Table 5); hence, the release kinetics must be diffusion controlled. Assuming the same diffusion coefficient as cesium in Ref. 4, a fractional release value of $N_d/N_{go} \sim 34\%$ is predicted with Eqs. (1) through (3). This prediction is in good agreement with the measured value in Table 4.

A similar calculation can also be performed for Ru and Ce. The previous value of the mass transfer coefficient ($k_m = 1.1$ mol m^{-2} s^{-1}) is a reasonable estimate for the other fission products since the diffusion coefficient in Eq. (16) will not change significantly. For instance, σ_{AB}^2 and $\Omega_{Ð_{AB}}$ are relatively constant at the higher boiling temperatures expected for the involatile species, and the inverse molecular weight of the fission product is much less than that of the gas atmosphere. An upper-bound of the vapor pressures can be immediately determined from the curves in Figs. 3 ($p_{H2}/p_{H2O} = 10$) and 4, respectively, where p_v (Ru) $= 3.98 \times 10^{-7}$ atm and p_v (Ce) $= 2.93 \times 10^{-8}$ atm. The results of the calculation are N_r (Ru) $= 1.8 \times 10^{17}$ atom and N_r (Ce) $= 1.3 \times 10^{16}$ atom. These values are orders of magnitude smaller than the original inventories (N_{go}) in Table 5 indicating, in this case, a vaporization-limited process. The corresponding release fractions (N_r/N_{go}) are again in good agreement with the measured results (see Table 4) where no significant release is observed.

As discussed in Section 2.2.2, the behaviour of Mo is much more complex. An estimate of the release fraction can be similarly performed, assuming there is no cesium in the gas atmosphere. Using the vapor pressure curves in either Fig. 3(a) or Fig. 5 (for $p_{H2}/p_{H2O} = 10$), p_v (Mo) $= 1.00 \times 10^{-5}$ atm, and therefore N_r (Mo) $= 4.6 \times 10^{18}$ atom. The vaporization release fraction is calculated as 0.9% using the original inventory in Table 5. This value is about a factor of 4 smaller than the measured release in Table 4. The present analysis is expected to provide a lower estimate since the effect of cesium is ignored in the calculation (see Fig. 5); however, this effect is less significant because the Cs_2MoO_4 will become unstable at higher temperature.

3.2.2 VERCORS-2 Test Analysis. The release kinetics of the volatile ^{134}Cs and ^{137}Cs species are shown in Fig. 8 for the VERCORS-2 test. The release does not start to increase until a temperature plateau of 1780 K is reached. At the high-temperature levels, the gas atmosphere is predominantly steam; however, the oxygen potential varied due to different trace quantities of hydrogen added to the carrier gas, i.e., p_{H2}/p_{H2O} = 0.018 (1780 K) and 0.18 (2100 K) (see Figs. 1 and 8). For the present analysis, the vapor pressures curves with $p_{H2}/p_{H2O} = 0.1$ are assumed.

The previous methodology of Section 3.2.1 can be applied, where now the bulk properties of the carrier gas are evaluated for a steam medium ($m_f = 25 \times 10^{-6}$ kg/s). The details of the calculation are provided in Table 6. For the polar steam molecule, a correction factor ξ, defined in Eq. (19), must be applied to the combining laws for the molecular potential parameters. In this analysis, the non-polar fission product is considered to be BaO for the given oxygen potential of the VERCORS-2 test (see Fig. 1). For a massive fission product present as a simple oxide compound, the polarizability can be reasonably approximated by the value for the elemental form; e.g., $\alpha_n = 39.7 \times 10^{-24}$ cm^3 for Ba.[22] Thus, using $t_p^* = 1.2$ for H_2O, the parameters in Table 6 follow where the parameter $\xi = 1.05$.

A laminar flow regime is again identified, leading to $Nu_{AB} = 4$. A corresponding mass transfer coefficient is calculated in Table 6 for the two high-temperature levels in Fig. 8. Similarly, using the vapor pressure curves with Eq. (6), the release fractions can be calculated for the various fission product species (see Table 4). In this calculation, the integral in Eq. (9) is carried out over 30 min at 1780 K and 13 min at 2100 K (see Fig. 8).

For the given test conditions, vaporization is the rate-limiting step for the release of Mo, Ce, Ru and Ba. The predicted release fractions for these species are in good agreement with the measured results, except for Mo that is again underpredicted by a similar factor of ~3. On the other hand, the volatile fission products (Cs, I, Xe) are controlled by diffusion through the fuel matrix (see Ref. 4).

3.3 Antimony and Tellurium Analysis

For the conditions in both CEA tests, the antimony and tellurium should be in a metallic state (see Fig. 1). Equilibrium thermodynamics indicate that the elemental forms of these species are very volatile so that diffusion would be the rate-limiting step.[8,13] However, as seen in Table 4, the release fraction of these isotopes are significantly smaller than those of the volatile species ^{137}Cs, ^{131}I and ^{135}Xe. This finding can be attributed to a chemical trapping of Te and Sb in the Zircaloy cladding that depends on the oxidation state of the cladding.[1,6,14] Tellurium (and barium) have been identified in the cladding material of the HEVA-6 specimen using a gamma-ray tomography technique (see Fig. 9).[23] It has been further suggested that the tellurium is trapped in the metallic Zircaloy as $ZrTe_2$.[1,6] More recent experiments have also provided evidence of trapping where the compound $Zr_{1+x}Te_2$ is formed at 723 to 1273 K; the zirconium-rich compound Zr_5Te_4 is favoured, however, at high-temperature (1273 K) in combination with a low tellurium vapor pressure.[24] During the clad-oxidation process, the tin constituent in the Zircaloy alloy is concentrated into a thin layer, producing a thermodynamically-stable species SnTe.[1,6] Since this species is volatile, a partial release of tellurium results.

The fission-product trapping can be empirically modelled as a reduced (diffusional) source release:

$$F = (1 - \zeta)\, F_d(\tau), \tag{26}$$

where ζ is a trapping fraction. An analysis of available CEA data indicates that the Te will be released when the clad is ~60% oxidized; however, limited data (for HEVA-6) suggest that the Sb will remain trapped until the oxidation process is complete. A small release of up to 18%, at a high temperature of 2700 K, was observed for the ORNL tests in a reducing atmosphere (VI-4 and VI-5), although this release may be attributed to the fact that the clad had melted and relocated in these experiments.[1] The fission-product trapping will also become less significant with increasing temperature. Using the end-of-test release fractions for Cs, Sb and Te, as measured in the HEVA/VERCORS test program (see Ref. 14), ζ (in %) can be correlated as a function of temperature (in K) and the clad oxidation state (see Fig. 10):

$$\zeta_{Sb} = 0, \quad (\mathit{clad\ oxidation} < 100\%)$$

$$\zeta_{Sb} = \begin{cases} 100, & T < 2001\ K, \\ -0.1817\,T + 463.6, & 2001 \le T \le 2551\ K, \quad (\mathit{clad\ oxidation} \sim 100\%) \\ 0, & T > 2551\ K, \end{cases} \tag{27}$$

$$\zeta_{Te} = 0, \quad (\mathit{clad\ oxidation} < 60\%)$$

$$\zeta_{Te} = \begin{cases} 100, & T < 1864\ K, \\ -0.1297\,T + 341.7, & 1864 \le T \le 2635\ K, \quad (\mathit{clad\ oxidation} \ge 60\%) \\ 0, & T > 2635\ K. \end{cases} \tag{28}$$

All tests in Fig. 10 experienced a pre-oxidative phase, i.e., the clad was completely oxidized in the VERCORS test series but only two-thirds oxidized in the HEVA-6 test. The correlation for tellurium in Eq. (28) follows from the measured release kinetics for ^{132}Te, and from the hydrogen production kinetics (as a result of Zircaloy oxidation) measured by gas chromatography. In the present analysis, a similar diffusion coefficient is implicitly assumed for Cs, Sb and Te; this assumption is supported by the observed release kinetics in Fig. 11, where the cladding was completely oxidized prior to any volatile fission-product release.

The model predictions for Sb and Te using Eqs. (26) through (28) are shown in Table 4. As expected, the calculations are in reasonable agreement with the measured results for the HEVA-6 and VERCORS-2 tests since the trapping correlation is derived in part from these data.

4. DISCUSSION

The present theoretical treatment is able to describe the release behaviour of both the volatile and involatile fission products (see Table 4). For the non-volatile species, the model is expected to be conservative; in the present representation (Section 2.2.1), it is assumed that the cladding does not offer any physical resistance. In reality, the mass transfer will occur in series (analogous to that of heat transfer), with an overall mass transfer coefficient defined by:[18]

$$\frac{1}{k_T} = \frac{1}{k_m} + \frac{1}{k_{clad}}, \tag{29}$$

in which k_{clad} accounts for the holdup effect of the cladding. In the present application (Section 3.2), it is implicitly assumed that $k_{clad} >> k_m$; alternatively, it can be seen in Eq. (29) that $k_T \leq k_m$, and therefore the use of k_m (rather than k_T) in Eq. (6) will result in an overprediction. This may help to explain the overestimation of the Ba-vaporization release in the VERCORS-2 test (see Table 4).

The present methodology can be applied to different flow conditions (e.g., turbulent flow or natural convection), and/or to other fuel geometries (e.g., a porous bed or fuel rod banks) with a suitable choice of the mass (heat) transfer coefficient (see, for example, Refs. 5 and 18). These cases may arise in various reactor accident scenarios. In addition, this work provides a means to extrapolate the test data for the given experimental conditions to those conditions found in the reactor (using an appropriate mass transfer coefficient).

For some species, the vapor pressure is somewhat dependent on the total system pressure and hydrogen-to-steam molar ratio. In particular, Mo is very sensitive to these parameters (see discussion in Section 2.2.2). A further free energy minimization analysis is therefore required to cover the full range of conditions of oxygen potential (hydrogen/steam gas mixtures) and total pressure (i.e., atmospheric pressure) experienced in the various annealing experiments. This is particularly important because the CEA and ORNL annealing tests form the majority of the data base for model validation. The extended calculation should also include the Eu species, which has been omitted in the earlier analysis of Refs. 7 to 9.

5. CONCLUSION

1. An analytical model has been developed to decribe the release behaviour of non-volatile fission products from uranium dioxide fuel during severe reactor accident conditions. The present treatment indicates that the release kinetics are dominated by the rate-controlling step for diffusional transport through the fuel matrix or vaporization from the fuel surface. The vaporization model is based on the equilibrium vapor pressure of the fission product and mass transport theory (for a laminar gas flow stream). The given vapor pressure was determined from an earlier free energy minimization calculation for a system consisting of a condensed phase (UO_2 plus fission products) and a gas phase (H_2O and H_2 plus gaseous fission products). An empirical correlation was also considered to account for the trapping of antimony and tellurium in the Zircaloy cladding as a function of temperature and the oxidation state of the clad.

2. Non-volatile release data were obtained in the CEA experiments, HEVA-6 and VERCORS-2, which were conducted, respectively, at high temperature (2370 K and 2150 K) in a hydrogen and steam atmosphere. The model is in agreement with the experimental results for the volatile (Cs, I and Xe), semi-volatile (Sb and Te), and non-volatile (Mo, Ce, Ru and Ba) fission product species.

ACKNOWLEDGEMENTS

The CEA experiments were supported by the Institut de Protection et de Sûreté Nucléaire (IPSN). The present analysis was supported by the CEA-Grenoble, the Royal Military College of Canada, and the Academic Research Program of the Department of National Defence of Canada (allocation no. 3705-882) and the Natural Sciences and Engineering Research Council of Canada (award no. OGP0155726).

REFERENCES

1. M.F. Osborne and R.A. Lorenz, "ORNL Studies of Fission Product Release Under LWR Severe Accident Conditions," Nucl. Safety 33 (1992) 344.

2. B.J. Lewis, D.S. Cox and F.C. Iglesias, "A Kinetic Model for Fission-Product Release and Fuel Oxidation Behaviour for Zircaloy-Clad Fuel Elements Under Reactor Accident Conditions," J. Nucl. Mater. 207 (1993) 228.

3. A.C. Harnden-Gillis, B.J. Lewis, W.S. Andrews, P.L. Purdy, M.F. Osborne and R.A. Lorenz, "Modeling of Cesium Release from Light Water Reactor Fuel Under Severe Accident Conditions," Nucl. Technol. 109 (1995) 39.

4. B.J. Lewis, B. Andre, B. Morel, P. Dehaudt, D. Maro, P.L. Purdy, D.S. Cox, F.C. Iglesias, M.F. Osborne and R.A. Lorenz, "Modelling the Release Behaviour of Cesium During Severe Fuel Degradation," J. Nucl. Mater., in press.

5. A.B. Reynolds, J.L. Kelly and S.T. Kim, "Role of Surface Vaporization in Low-Volatility Fission Product Release Experiments," Nucl. Technol. 74 (1986) 76.

6. R.R. Hobbins, D.A. Petti and D.L. Hagrman, "Fission Product Release From Fuel Under Severe Accident Conditions," Nucl. Technol. 101 (1993) 270.

7. D. Cubicciotti, "Vaporization Thermodynamics of Fission Products from Fuel Under Nuclear-Accident Conditions," Advances in Ceramics, Vol. 17, American Ceramic Society, Columbus, Ohio, 1986, p. 211.

8. D. Cubicciotti and B.R. Sehgal, "Vapor Transport of Fission Products in Postulated Severe Light Water Reactor Accidents," Nucl. Technol. 65 (1984) 267.

9. D. Cubicciotti, "Vapor Transport of Fission Products Under Nuclear Accident Conditions," J. Nucl. Mater. 154 (1988) 53.

10. M. Ramamurthi and M.R. Kuhlman, "Refinement of CORSOR - An Empirical In-Vessel Fission Product Release Model," U.S. Nuclear Regulatory Commission, Battelle report, 1990.

11. T.B. Reed, "Free Energy of Formation of Binary Compounds: An Atlas of Charts for High-Temperature Chemical Calculations," MIT Press Cambridge, Massachusetts, 1971.

12. M.W. Chase, C.A. Davies, J.R. Downey, D.J. Frurip, R.A. McDonald and A.N. Syverud, "JANAF Thermochemical Tables," Third Edition, Journal of Physical and Chemical Reference Data, Vol. 14, 1985, Supplement No. 1.

13. I. Barin, "Thermochemical Data of Pure Substances," VCH Publishers, New York, 1989.

14. B. Andre, G. Ducros, J.P. Leveque, D. Maro, M.F. Osborne and R.A. Lorenz, "Fission Product Releases at Severe LWR Accident Conditions: ORNL/CEA Measurements Versus Calculations," submitted to Nucl. Technol.

15. J.P. Leveque, B. Andre, G. Ducros, G. Le Marois and G. Lhiaubet, "The HEVA Experimental Program," Nucl. Technol. 108 (1994) 33.

16. P.E. Blackburn, "Oxygen Pressures over Fast Breeder Reactor Fuel, (I) A Model for $UO_{2\pm x}$," J. Nucl. Mater. 46 (1973) 244.

17. V.J. Wheeler and I.G. Jones, "Thermodynamic and Composition Changes in $UO_{2\pm x}$ ($x < 0.005$) at 1950 K," J. Nucl. Mater. 42 (1972) 117.

18. R.B. Bird, W.E. Stewart and E.N. Lightfoot, "Transport Phenomena," John Wiley & Sons, New York (1960).

19. L.S. Tong and J. Weisman, "Thermal Analysis of Pressurized Water Reactors," American Nuclear Society, 1979, p. 279.

20. R.C. Reid and T.K. Sherwood, "The Properties of Gases and Liquids," second edition, McGraw-Hill, New York (1966).

21. J.O. Hirschfelder, C.F. Curtiss and R.B. Bird, "Molecular Theory of Gases and Liquids," John Wiley & Sons, New York (1964).

22. D.R. Lide, "CRC Handbook of Chemistry and Physics," 72nd edition, CRC Press, 1991.

23. J.P. Leveque, G. Lhiaubet and B. Boulaud, "HEVA Experimental Programme: Final Report," Commissariat à l'Energie Atomique, technical report DPEI/SEAC No. 91/08, November 1991.

24. R. de Boer and E.H.P. Cordfunke, "Reaction of Tellurium with Zircaloy-4," J. Nucl. Mater. 223 (1995) 103.

TABLE 1: INTERMOLECULAR FORCE PARAMETERS FOR VARIOUS CARRIER GAS CONSTITUENTS

Substance	Molecular Weight M (g/mol)	Lennard-Jones Parameters		Reference
		σ (Å)	ϵ/κ (K)	
H_2	2.016	2.915	38.0	18
He	4.003	2.576	10.2	18
H_2O	18.015	2.65	380	21

TABLE 2: MOLES OF FISSION PRODUCTS USED IN SOLGASMIX ANALYSIS

Fuel Burnup of 42800 MWd/tU$^{(a)}$ (4.5 atom% burnup)		Fuel Burnup of 37000 MWd/tU$^{(b)}$	
Element	Moles	Element	Moles
Zr	3440	Sr	860
Nb	33	Ba	945
Mo	3150	Y	446
Tc	754	La	825
Ru	2270	Ce	1820
Rh	263	Pr	734
Pd	1360	Nd	2340
U	264000	U	264000

(a) Taken from Ref. 7. Distribution of fission products assumed in analysis of Fig. 3.
(b) Taken from Ref. 9. Distribution of fission products assumed in analysis of Fig. 4.

TABLE 3: SUMMARY OF EXPERIMENTAL PARAMETERS FOR HEVA-6 AND VERCORS-2 TESTS

Parameter	HEVA-6[a]	VERCORS-2[a]
Test description	- Fission Product Release at 2370 K in H_2 with irradiated/re-irradiated fuel - Aerosol sizing at 520 K	- Fission Product Release at 2150 K in H_2O and H_2 with irradiated/re-irradiated fuel - Aerosol sizing at 870 K
Fuel specimen		
Fuel type	Fessenheim 1/2	Bugey/3
Rod identification	C12 (FDC 57)	C19 (FGC 53)
Enrichment (wt% ^{235}U)	3.1	3.1
Clad Outer Diam. (mm)	9.50	9.50
Pellet Outer Diam. (mm)	8.19	8.19
Pellet length (mm)	13.96	13.96
Fissile length (mm)	46	44
Sample height (mm)	80	80
Irradiation Data		
Irradiation period	3 cycles to 06/81	3 cycles to 02/83
Burnup (MWd/kgU)	36.7	38.3
Average heat rating (W/cm)	185	-
Cooling period (y)	7	7
Grain radius (μm)	7.5	7.5
Re-irradiation	Yes	Yes
Test conditions		
Test date	3/88	6/90
Temperature rise (K/s)	1.4	1.6
Maximum temperature (K)	2370	2150
Time at high-temperature plateau (s)	1800	780
Flow rate (mg/s)		
H_2	0.2	0.5
H_2O	0	25
Impactor temperature (K)	520	870
Ag/In/Cd	No	No

(a) Taken from Ref. 4.

TABLE 4: COMPARISON BETWEEN MEASURED AND PREDICTED RELEASE FRACTIONS

Chemical species	HEVA-6				VERCORS-2			
	Measured[a]		Predicted		Measured[a]		Predicted	
	Isotope	Fractional release (%)		Rate-limiting step[c]	Isotope	Fractional release (%)		Rate-limiting step[c]
Cs	137	30	34[b]	SD	137, 134	29, 32	41[b]	SD
I	131	30	34[b]	SD	131	24	41[b]	SD
Xe	135	15	34[b]	SD	135	~22	41[b]	SD
Te	132	11	20[b]	SD+ZT	132	19	13[b]	SD+ZT
Sb	127	0	0[b]	SD+ZT	125	~7	7[b]	SD+ZT
Mo	99	~4	0.9	VLP	99	17	5	VLP
Eu	154	~5	-	-	154	~0	-	-
Ce	143	0	0.005	VLP	144	~0	0.00004	VLP
Ru	103	0	0.04	VLP	106	~0	0.003	VLP
Ba	140	27	34[b]	SD	140	≤8	17	VLP

(a) Taken from Ref. 4.

(b) Predicted for diffusional release kinetics where $D_{Cs} = D_I = D_{Xe} = D_{Ba} = D_{Sb} = D_{Te}$ and using the diffusion coefficient for cesium in Ref. 4. For Sb and Te, the trapping effects in the Zircaloy cladding are calculated in accordance with Eqs. (26) through (28).

(c) SD = Solid Diffusion; VLP = Vaporization-Limited Process; ZT = Zircaloy Trapping.

TABLE 5: INITIAL FISSION PRODUCT INVENTORY IN CEA TESTS

Element	Inventory N_{go} (atom)(a)	
	HEVA-6	VERCORS-2
Br	4.67×10^{18}	3.58×10^{18}
Kr	5.92×10^{19}	5.74×10^{19}
Rb	5.87×10^{19}	5.69×10^{19}
Sr	1.27×10^{20}	1.22×10^{20}
Mo	5.14×10^{20}	4.99×10^{20}
Ru	4.54×10^{20}	3.14×10^{20}
Sb	3.74×10^{18}	1.24×10^{18}
Te	5.57×10^{19}	5.38×10^{19}
I	2.76×10^{19}	2.63×10^{19}
Xe	6.06×10^{20}	5.90×10^{20}
Cs	2.67×10^{20}	2.51×10^{20}
Ba	1.41×10^{20}	1.37×10^{20}
La	1.30×10^{20}	1.27×10^{20}
Nd	3.66×10^{20}	3.52×10^{20}
Ce(b)	2.85×10^{20}	2.74×10^{20}

(a) Based on calculations with the MARISE code.
(b) Calculated using the ratio of Ce/Nd in Table 2.

TABLE 6: CALCULATION OF VAPORIZATION-MODEL PARAMETERS FOR VERCORS-2

Parameters	Temperature	
	1780 K	2100 K
Bulk Properties		
Density, ρ (kg/m^3)	0.123	0.105
Viscosity, μ (kg m^{-1} s^{-1})(a)	7.10×10^{-5}	8.02×10^{-5}
Ω_μ	0.96	0.92
Flow Velocity, V (m/s)	0.48	0.57
Diffusion Coefficient, $Đ_{AB}$ (m^2/s)(a,b)	1.52×10^{-4}	2.07×10^{-4}
$\Omega_{ĐAB}$	1.24	1.17
Reynolds number, Re	13	12
Schmidt number, Sc	3.78	3.71
$L/(DReSc)$	0.105	0.121
Mass Transfer Coefficient		
$cĐ_{AB}$ (mol m^{-1} s^{-1})	1.043×10^{-3}	1.200×10^{-3}
k_m (mol m^{-2} s^{-1})	0.269	0.310

(a) Assumes $\sigma_B = 2.65$ Å and $\epsilon/\kappa = 380$ K for H_2O.
(b) Assumes $\sigma_A = 6.0$ Å and $\epsilon/\kappa = 3680$ K for BaO (see Section 3.2.1).

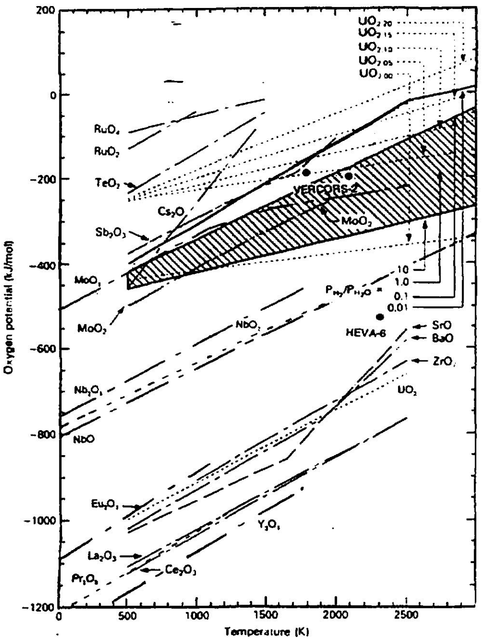

FIGURE 1. Oxygen potential plotted against temperature for fission product oxides, UO_{2+x} and hydrogen/steam gas atmospheric mixtures. The oxygen potentials of the HEVA-6 and VERCORS-2 tests (solid circles) are also shown.

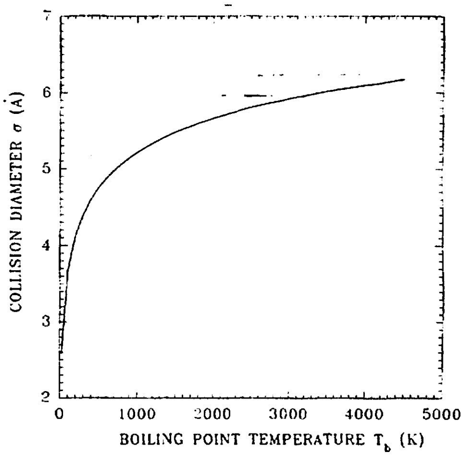

FIGURE 2. Collision diameter (σ) versus boiling point temperature (T_b).

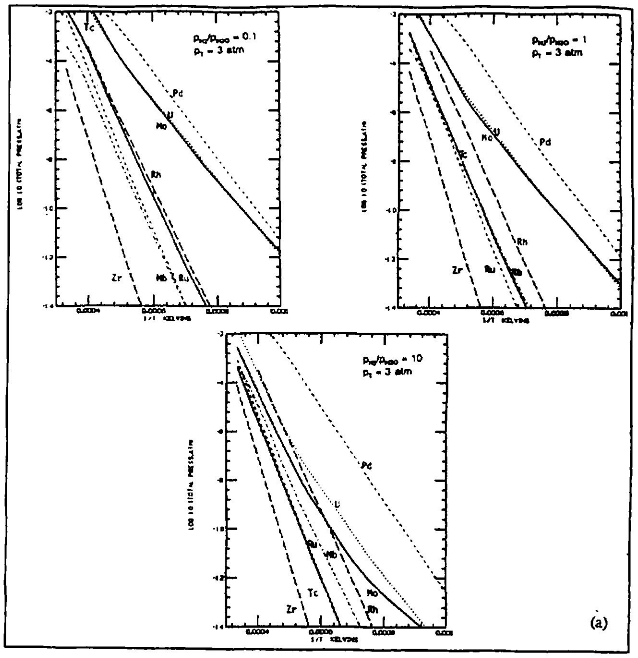

Element	Constants for Simplified Equation			
	A_1	A_2	B_1	B_2
Zr	9.77	0.03	42 200	-92
Nb	6.28	-0.25	28 600	-750
Tc	7.52	-0.19	30 500	1830
Ru	8.25	-0.28	32 900	520
Rh	6.98	0.15	27 000	360
Pd	6.03	0.26	18 000	900
Equation:	$\mathrm{Log}(p_v,\mathrm{atm}) = [A_1 + A_2\,\mathrm{Log}(p_{H2}/p_{H2O}) - (B_1 + B_2\,\mathrm{Log}(p_{H2}/p_{H2O}))/T]$ (b)			

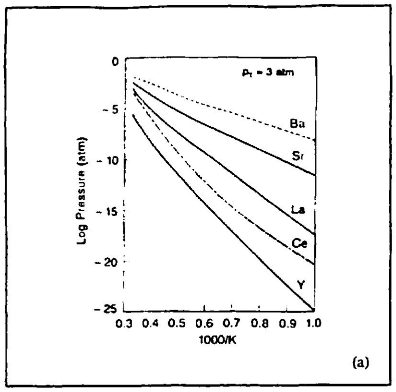

Element	Constants for Simplified Equation		
	A	B	C
Sr	-13 800	2.0	0.006
Ba	-9 600	1.3	0.007
La	-21 000	3.4	0.008
Ce (Nd, Pr)	-24 300	4.18	0.001
Y	-23 000	1.14	0.007
Equation:	$\mathrm{Log}(p_v,\mathrm{atm}) = A/T + B + C\,p_T\,(\mathrm{atm})$ (b)		

FIGURE 4. Fission product vapor pressures of Ba, Sr, La, Ce, Nd, Pr and Y. The given results are for $p_{H2}/p_{H2O} = 1$. The curves for $p_{H2}/p_{H2O} = 0.1$ and 10 are very similar. (Taken from Ref. 9.)

(a) Curves from Solgasmix analysis.

(b) Simplified equations of vapor pressure curves.

FIGURE 3. Fission product vapor pressures of Zr, Nb, Mo (no cesium present), Tc, Ru, Rh, Pd (and U). (Taken from Ref. 7.)

(a) Curves from Solgasmix analysis.

(b) Simplified equations of vapor pressure curves.

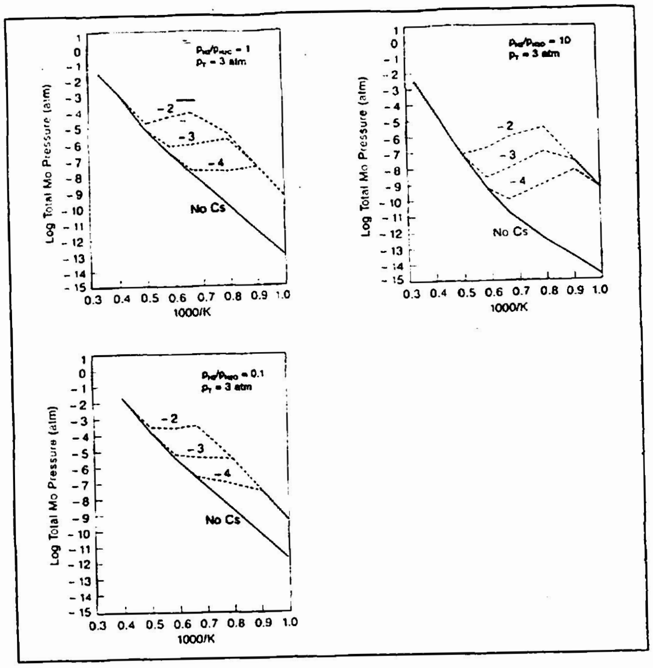

FIGURE 5. Vapor pressures of Mo calculated by Solgasmix analysis. For each curve, the log of the total cesium pressure is indicated. (Taken from Ref. 9.)

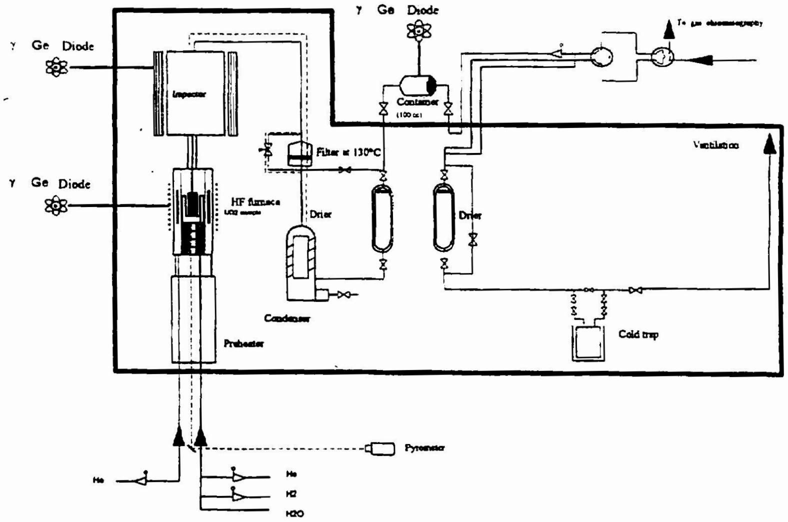

FIGURE 6. HEVA/VERCORS experimental facility at the CEA.

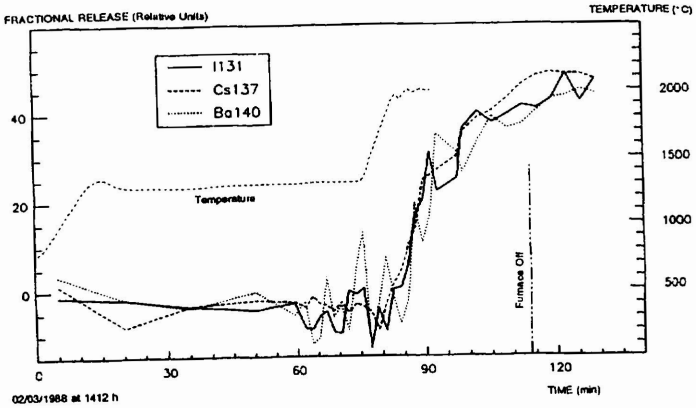

FIGURE 7. Measured release kinetics of ^{131}I, ^{137}Cs and ^{140}Ba for the HEVA-6 test. The temperature profile history is also shown.

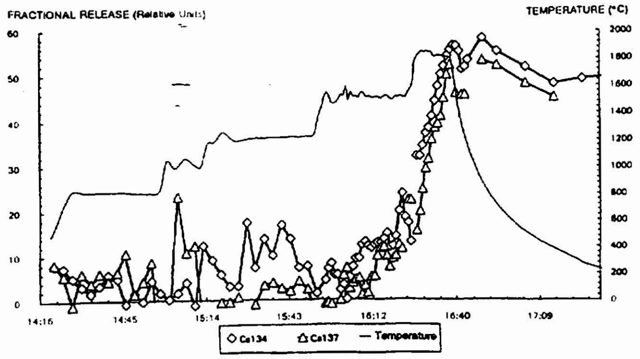

FIGURE 8. Measured release kinetics of ^{134}Cs and ^{137}Cs for the VERCORS-2 test. The temperature profile history is also shown.

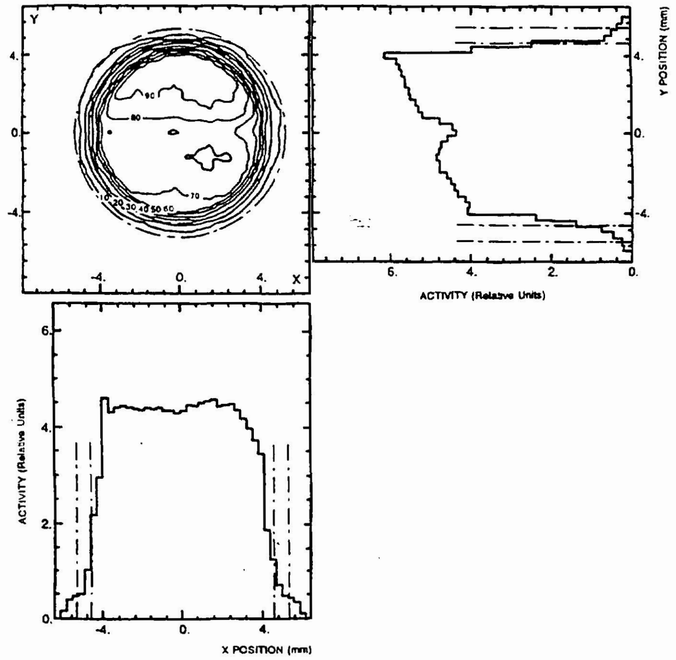

FIGURE 9. Distribution of ^{132}Te in the fuel rod and cladding for the HEVA-6 test using gamma-ray tomography. (Taken from Ref. 23.)

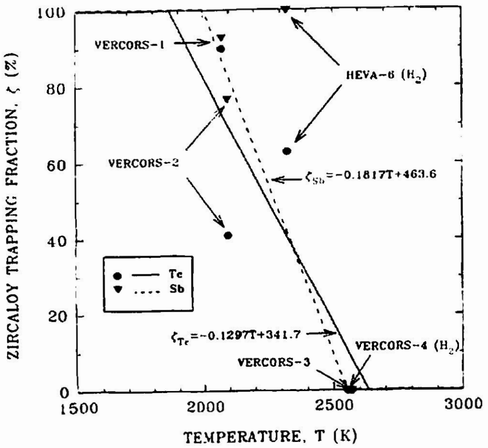

FIGURE 10. Correlation of trapping fraction (ζ) for Sb and Te in Zircaloy cladding as a function of temperature (T).

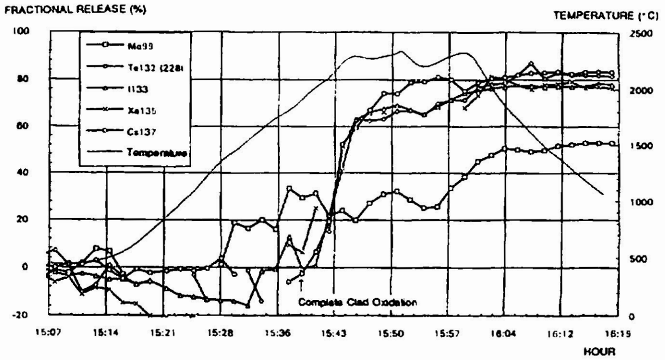

FIGURE 11. Measured release kinetics of ^{99}Mo, ^{132}Te, ^{133}I, ^{135}Xe and ^{137}Cs for the VERCORS-3 test. The temperature profile history is also shown.